Attribution of Projected Future Changes in Tropical Cyclone Passage Frequency over the Western North Pacific

SATORU YOKOI AND YUKARI N. TAKAYABU

Atmosphere and Ocean Research Institute, University of Tokyo, Kashiwa, and Japan Agency for Marine–Earth Science and Technology, Yokosuka, Japan

HIROYUKI MURAKAMI

Japan Agency for Marine–Earth Science and Technology, Meteorological Research Institute, Tsukuba, Japan

(Manuscript received 22 April 2012, in final form 21 November 2012)

ABSTRACT

This paper performs an attribution analysis of future changes in the frequency of tropical cyclone (TC) passages over the western North Pacific basin projected by seven general circulation models. The models project increases in the passage frequency over the tropical central North Pacific and decreases in regions to the west and northwest, including East Asian countries. The attribution analysis reveals that while changes of the basinwide TC count would decrease the frequency of passages throughout the basin, the gross horizontal contrast in the passage frequency changes is caused by a projected eastward shift of main TC development regions, probably caused by El Niño–like sea surface temperature changes. The change in the frequency of passages is also caused by changes of TC translation vectors and preferable tracks. In particular, the translation vector would rotate clockwise to point in a more easterly direction over oceanic regions south of Japan, decreasing the passage frequency over the Korean peninsula and western Japan while increasing it over eastern Japan. This change in translation direction may be caused by the southward shift of the subtropical jet axis and resultant intensification of westerly steering flows. The El Niño–like change and westerly steering flow change are consistent not only among the seven models but also among a number of other climate models, which suggests the reliability of these results from the viewpoint of intermodel agreement.

1. Introduction

Tropical cyclones (TCs), known as typhoons in the western North Pacific (WNP) basin (0°–40°N, 100°E–180°), are among the most devastating atmospheric disturbances, causing torrential rainfall, strong winds, and storm surges in coastal nations. Because of the severity of their potential impacts, there have been numerous efforts to project the impacts of global warming on TC activity through the so-called direct approach. In this approach, we detect and track TC-like vortex disturbances simulated in present and future climate experiments by general circulation models (GCMs) and compare their behavior between the two experiments. Knutson et al. (2010) summarized projections from a number of recent studies. They pointed out that most recent studies project decreases in the global TC count (e.g., Sugi et al. 2002; Oouchi et al. 2006; Gualdi et al. 2008; Zhao et al. 2009; Sugi et al. 2009); however, projections of the TC count over individual ocean basins are not as consistent among the studies.

Compared with the global and ocean basinwide counts, future projections of TC landfall frequency in individual affected regions is a more direct concern for local populations. While we can also obtain the projections of such regional passage frequency through the direct approach as done, for example, by Murakami et al. (2011, 2012b), it is more complicated to discuss their causes and evaluate their reliability compared with the TC count projections. This is because the passage frequency is influenced by several aspects of the statistical

Corresponding author address: Satoru Yokoi, Japan Agency for Marine–Earth Science and Technology, 2-15, Natsushima-cho, Yokosuka, Kanagawa 237-0061, Japan.
E-mail: yokoi@jamstec.go.jp

DOI: 10.1175/JCLI-D-12-00218.1

TABLE 1. List of GCMs examined in this study.

ID	Model Acronym	Model Expansion	Type	Resolution (km)	Reference
A	MRI-AGCM3.1S	Meteorological Research Institute (MRI) Atmospheric General Circulation Model, version 3.1S	AGCM	~20	Mizuta et al. (2006)
B	MRI-AGCM3.2S	Meteorological Research Institute Atmospheric General Circulation Model, version 3.2S	AGCM	~20	Mizuta et al. (2012)
C	CGCM3.1 (T63)	Canadian Centre for Climate Modelling and Analysis (CCCma) Coupled Global Climate Model, version 3.1 (T63)	AOGCM	~310	Flato et al. (2000)
D	CSIRO Mk3.0	Commonwealth Scientific and Industrial Research Organisation (CSIRO) Mark, version 3.0	AOGCM	~210	Gordon et al. (2002)
E	CSIRO Mk3.5	CSIRO Mark, version 3.5	AOGCM	~210	Gordon et al. (2002)
F	INGV-SXG	Instituto Nazionale di Geofisica e Vulcanologia (INGV) SINTEX-G	AOGCM	~120	Gualdi et al. (2008)
G	ECHAM5/MPI-OM	ECHAM5/Max Planck Institute for Meteorology (MPI) Ocean Model	AOGCM	~210	Roeckner et al. (2003)

behavior of the TCs. First, the future change in the basinwide TC count (BC) affects the regional passage frequency. Changes in the spatial distribution of the genesis frequency in the basin [genesis distribution (GD)] also influence the passage frequency, because the preferable track (PT) usually taken by TCs after their formation depends strongly on their genesis locations. Furthermore, the PT would shift in the future climate, which also leads to passage frequency trends. The future changes of these three aspects (BC, GD, and PT) each result from different causes, and each is subject to uncertainty. To discuss the causes and reliability of changes in passage frequency, it seems necessary to clarify the parts of changes caused by BC, GD, and PT. Such attribution analysis of the passage frequency changes has never been attempted in previous studies.

Recently, Yokoi and Takayabu (2013, hereafter YT) proposed the Integration of Statistics on TC Activity by Genesis Location (ISTAGL) analysis through which differences in the passage frequency between two track datasets can be decomposed into contributions of differences in BC, GD, and PT. Using this method, they discussed the causes of the decadal variability of passage frequency over the WNP. They further noted that this method may also help in future projection studies.

The main objective of the present study is to apply the ISTAGL analysis to simulated track data of the current and future climate from seven GCMs, obtained from previous studies of the authors (Yokoi et al. 2009; Yokoi and Takayabu 2009; Murakami et al. 2011, 2012b), to discuss the causes and reliability of the simulated passage frequency changes over the WNP. Through presentation of this analysis, we want to emphasize the effectiveness of the attribution analysis for a better understanding of the passage frequency changes and to show the performance of the ISTAGL analysis.

The rest of this paper is organized as follows. In section 2, we document simulated TC track data and observed best-track data. We then explain the methodology of the ISTAGL analysis. In section 3a, we evaluate the models' performance in simulating passage frequency and discuss the attribution of model biases. Then, in section 3b, we perform a multimodel-based future projection and its attribution. In sections 3c and 3d, we discuss possible physical mechanisms responsible for projected future changes in the passage frequency. Finally, section 4 presents conclusions of this study.

2. Data and method

a. TC track data

In this study, we perform a multimodel-based future projection by analyzing TC track data simulated by seven GCMs, which are listed in Table 1 (additional models involved in this study are provided in Table 2). The multimodel approach has been increasingly recognized as a necessary method for evaluating and reducing uncertainties that are inevitable for future projections.

Two GCMs (A and B; Tables 1 and 2 provide the models associated with each ID) are atmosphere-only GCMs (AGCMs) with horizontal resolutions that are as high as 20 km, developed at the Meteorological Research Institute (MRI), Japan. A detailed description of these models is provided by Mizuta et al. (2006, 2012). The main difference between the two models is the cumulus parameterization scheme. Murakami et al. (2011, 2012b) detected and tracked TC-like disturbances simulated in current and future climate experiments of models A and B, respectively. Both experiments have 25-yr length. The boundary conditions used by the current

TABLE 2. Acronyms and expansions of additional GCMs involved in this study.

ID	Model Acronym	Model Expansion
H	BCCR-BCM2.0	Bjerknes Centre for Climate Research Bergen Climate Model, version 2.0
I	CCSM3.0	Community Climate System Model, version 3.0
J	CGCM3.1 (T47)	Canadian Centre for Climate Modelling and Analysis Coupled Global Climate Model, version 3.1 (T47)
K	CNRM-CM3	Centre National de Recherches Météorologiques Coupled Global Climate Model, version 3
L	FGOALS-g1.0	Flexible Global Ocean–Atmosphere–Land System Model gridpoint, version 1.0
M	GFDL-CM2.0	Geophysical Fluid Dynamics Laboratory Climate Model, version 2.0
N	GFDL-CM2.1	Geophysical Fluid Dynamics Laboratory Climate Model, version 2.1
O	GISS-AOM	Goddard Institute for Space Studies, Atmosphere–Ocean Model
P	GISS-EH	Goddard Institute for Space Studies Model E, coupled with the HYCOM ocean model
Q	GISS-ER	Goddard Institute for Space Studies Model E-R
R	INM-CM3.0	Institute of Numerical Mathematics Coupled Model, version 3.0
S	IPSL-CM4	L'Institut Pierre-Simon Laplace Coupled Model, version 4
T	MIROC3.2 (hires)	Model for Interdisciplinary Research on Climate, version 3.2 (high resolution)
U	MRI-CGCM2.3.2a	Meteorological Research Institute Coupled Atmosphere–Ocean General Circulation Model, version 2.3.2a
V	HadCM3	Hadley Centre Coupled Model, version 3

climate experiment are observed monthly sea surface temperature (SST), sea ice concentration, and greenhouse gas concentrations for the period 1979–2003. Those used by the future climate experiment are trends of SST and sea ice concentration estimated from multimodel ensemble of the third phase of the Coupled Model Intercomparison Project (CMIP3; Meehl et al. 2007a) under the Special Report on Emissions Scenarios (SRES) A1B scenario superimposed on the observations, as well as the greenhouse gas concentrations taken from the SRES A1B scenario. These experiments were performed in order to contribute to the fifth phase of the Coupled Model Intercomparison Project (CMIP5; Taylor et al. 2012).

The other five GCMs (C–G) are atmosphere–ocean coupled GCMs (AOGCMs) that participated in CMIP3. Yokoi et al. (2009) and Yokoi and Takayabu (2009) detected and tracked TC-like disturbances from the daily outputs of twentieth-century climate experiments with 40-yr (1961–2000) lengths and those of future climate experiments using the SRES A1B scenario with 40-yr (2046–65 and 2081–2100) lengths. The daily outputs are archived at the Program for Climate Model Diagnosis and Intercomparison (PCMDI) database. Among more than 20 CMIP3 AOGCMs, Yokoi et al. (2009) examined the performance of eight models (including these five models), because their daily outputs are available at the database and their horizontal resolutions are T63 or greater. Yokoi et al. (2009) demonstrated that these five models have higher performance in simulating the horizontal distribution of TC genesis over the WNP basin than the other three models, and thus were utilized for the multimodel projection of future genesis frequency in Yokoi and Takayabu (2009). Note that they did not examine the passage frequency changes.

For the direct approach, we have to determine detection criteria of the TC-like vortex disturbances, mainly based on the existence of lower-tropospheric cyclonic vorticity and upper-tropospheric warm core structure. Details of the criteria differ from one study to another. Murakami et al. (2011, 2012b) adopt more complicated criteria than Yokoi et al. (2009). Because different models adopt different specifications, such as horizontal resolution and parameterization schemes, it is desirable to determine threshold values for the criteria independently for each model. Generally speaking, when we adopt stricter threshold values, the number of detected disturbances may decrease and their genesis location may shift northwestward, and vice versa. Therefore, Yokoi et al. (2009) tuned threshold values for each model so that latitudinal distribution of annual genesis frequency over the WNP is the closest to the observations. The threshold values adopted by Murakami et al. (2012b) also differ from those by Murakami et al. (2011).

To evaluate the models' performance, we compare the simulated passage frequency with the TC best-track data issued by the Regional Specialized Meteorological Center Tokyo–Typhoon Center, Japan Meteorological Agency, for the 25-yr period of 1979–2003. The dataset provides the positions of the TC centers and their intensities every 6 h. In this paper, the TC genesis location is defined as the first position where the maximum 10-min mean sustained wind speed exceeds 17.5 $\mathrm{m\,s^{-1}}$, which is known as tropical storm (TS) strength. The TCs are tracked until they experience extratropical transition or lose TS strength.

We should note that we examine future projection of only seven GCMs and thus the multimodel approach can cover only a small portion of intermodel diversity of dozens of GCM experiments performed under the CMIP3 and its subsequent projects. Therefore, it seems

premature to argue for the reliability of future changes from the viewpoint of intermodel consistency even if the seven models project the same tendency of the changes. However, examination of the direct approach using all of the CMIP3 AOGCMs is difficult because of the coarse horizontal resolution or the lack of daily outputs for most of the models. Instead, to bolster the reliability of projected changes in the passage frequency that are consistent among the seven models, we will discuss the intermodel consistency of future changes of environmental conditions that are considered to be responsible for the passage frequency change, which we can assess using outputs of many more CMIP3 AOGCMs listed in Table 2.

b. Decomposition method

As explained in the introduction, the future change in passage frequency is caused by changes in the BC, GD, and PT. YT proposed a method of decomposing passage frequency changes into contributions of these three aspects of the statistical behavior of TCs and referred to it as the ISTAGL analysis. In this method, we express the passage frequency over an area A for a certain period as

$$F(A) = C \iint g(A_g) \times p(A \mid A_g)\, dA_g, \qquad (1)$$

where $F(A)$ is the passage frequency, C is the BC, $g(A_g)$ is the genesis frequency over an area A_g divided by C, and $p(A \mid A_g)$ is the probability that TCs generated in A_g pass over A. The basic idea under this transformation is that the PT that TCs tend to take depends strongly on their genesis location. Using this equation, the difference in the passage frequency between two TC track datasets F' can be expressed as

$$F' = C' \iint g_R p_R\, dA_g + C_R \iint g' p_R\, dA_g + C_R \iint g_R p'\, dA_g + \mathrm{NL}, \qquad (2)$$

where subscript R represents the variables of the reference track data and the prime represents differences of the target track data with respect to the reference data. This equation represents the decomposition of the passage frequency difference. The first, second, and third terms on the right-hand side represent contributions from differences in BC, GD, and PT, respectively, with other factors unchanged. The last term NL is the sum of the nonlinear terms with respect to these three differences. Note that we can obtain all variables that appeared in Eq. (2), and thus the four contribution terms, directly from the track datasets.

Using this approach, YT demonstrated that the decadal variability in the passage frequency over the WNP basin was successfully decomposed into the four contribution terms. They revealed that the PT contribution played the most essential role in the decadal variability over the midlatitudes, while the BC and GD contributions also influenced the variability over the subtropics. Although it appears to be necessary to analyze an appropriately large number of TC samples to accurately estimate the variables in Eq. (2), results reported by YT imply the applicability of this method to passage frequency variability with decadal and longer time scales over the WNP basin. Furthermore, they noticed that the NL contribution is so small that, for a first approximation, the decadal-scale passage frequency variability can be considered on a linear framework of the BC, GD, and PT contributions.

In this study, we adopt $10° \times 10°$ grid boxes embedded in the WNP basin for A_g and $2.5° \times 2.5°$ grid boxes for A. To reduce the dependency of decomposition results on the configuration of A_g grid boxes, we shift these boxes by 2.5°, 5°, and 7.5° longitudinally and latitudinally to repeat the analysis (in total, 16 calculations) to confirm that the results presented in this paper are qualitatively insensitive to the grid shifts. In this paper, we present the averages of the results obtained from these 16 calculations.

In section 3a, we use Eq. (2) to attribute biases in the simulated passage frequency by setting the observed track data as the reference data and the simulated track data as the target data. Then, we use this equation in section 3b to attribute the projected future change by setting the track data in the current climate experiment as the reference data and those in the future climate experiment as the target data. The target season in this study is the July–September period, which is the most active period for TCs in the WNP basin. During this period, observed GD and PT do not change significantly, as demonstrated in YT, and neither does the large-scale environmental circulation field (LinHo and Wang 2002).

3. Results and discussion

a. Model biases

In this section, we evaluate the models' performances in simulating the horizontal distribution of the passage frequency and discuss the attribution of its bias using the ISTAGL analysis. Figure 1 compares the simulated and observed passage frequencies. The passage frequency is calculated with the $2.5° \times 2.5°$ grid boxes, and smoothed longitudinally and latitudinally using a 1–2–1 spatial filter. The observed frequency (Fig. 1h) is highest over

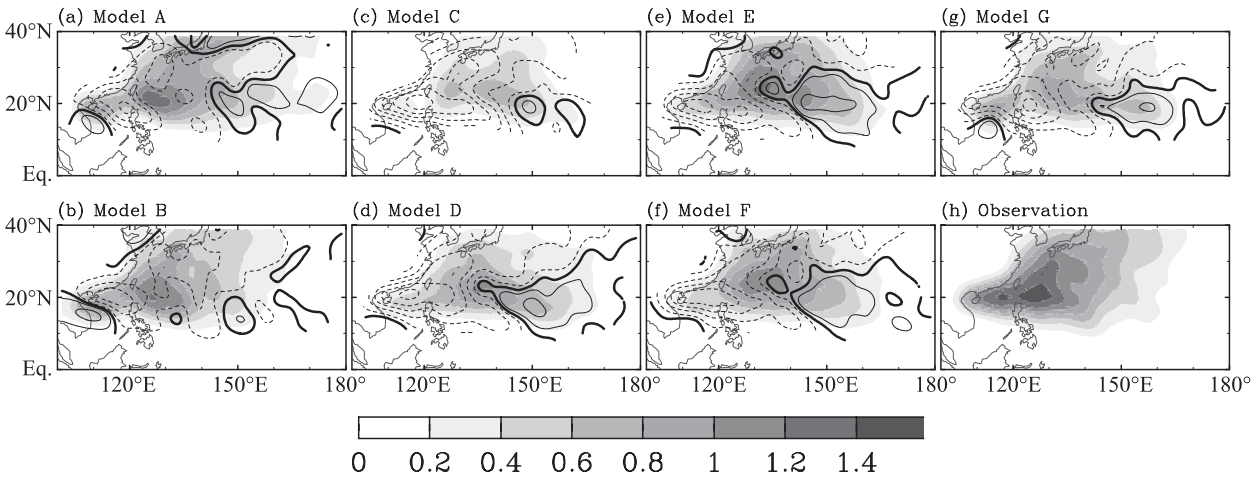

FIG. 1. (a)–(g) Passage frequency in the July–September season simulated by individual models by gray and its bias with respect to the observation by and (h) observed passage frequency in the same season of 1979–2003. The unit of the frequency is number of TCs over a 2.5° × 2.5° area for a 3-month season. Thick solid contours denote zero, and thin solid (dashed) contours indicate positive (negative) biases, starting with ±0.1, with an interval of 0.2. A 1–2–1 spatial smoothing has been applied each in longitudinal and latitudinal directions.

the northern South China Sea (SCS) and the Philippine Sea southeast of Taiwan, whereas it is considerably lower in the equatorial region and the eastern part of the basin. In the midlatitudes, a ''ridge'' of high frequency extends in a north-northeastward direction from the subtropics into western Japan. While the models broadly reproduce such spatial contrast, there are some biases shown by contours. Most models underestimate the passage frequency in the northern SCS, Philippine Sea, and midlatitudes, and several models overestimate it in the eastern part of the domain along 20°N.

The reproducibility of the horizontal distribution of the passage frequency by the seven models is measured by an S index proposed by Taylor (2001), which is expressed as

$$S = \frac{(1 + r_{so})^4}{4(\sigma_s/\sigma_o + \sigma_o/\sigma_s)^2},$$

where σ_s and σ_o are the spatial standard deviations of the simulated and observed passage frequencies, respectively, and r_{so} is the spatial correlation coefficient between the two passage frequencies. These statistics are evaluated over the entire WNP basin. This index ranges from 0 to 1; higher values indicate closer similarities between the simulated and the observed passage frequencies, and thus, higher reproducibility of the model. The S indices for individual models are shown in the third column of Table 3. Two MRI AGCMs (A and B) exhibit higher performance than the five CMIP3 AOGCMs (C–G). The higher performance of the AGCMs is partially because that they have much higher horizontal resolutions than the CMIP3 models, and this is believed to be important for an improved simulation of TCs. Another probable reason is that the AOGCMs have to simulate the SST distribution, which is sometimes biased and can cause a bias in the environmental circulation fields that influence the reproducibility of TC behavior. In contrast, the AGCMs are expected to be able to reproduce the circulation field more realistically because the SST distribution is given as the boundary condition.

The passage frequency bias can be decomposed into BC-, GD-, and PT-bias contributions and the NL contribution by setting the observations as the reference and the simulations as the target data in the ISTAGL analysis. The decomposition of the biases is presented in Fig. 2. The BC bias causes an overall negative bias of the passage frequency for all of the models, although the magnitude of the BC bias for model A is so small that

TABLE 3. Observed (Obs.) and simulated (model IDs A–G) BC in the July–September season; model performance in simulating passage frequency distribution measured by the Taylor (2001) S index; RMSE of F', BC bias, GD bias, PT bias, and NL contributions.

			RMSE				
ID	BC	S index	F'	BC	GD	PT	NL
Obs.	14.3						
A	13.8	0.75	0.39	0.05	0.18	0.32	0.01
B	10.9	0.77	0.38	0.29	0.08	0.23	0.06
C	6.7	0.35	0.80	0.65	0.36	0.39	0.34
D	9.7	0.52	0.63	0.40	0.32	0.36	0.19
E	11.2	0.70	0.47	0.27	0.26	0.29	0.15
F	10.7	0.68	0.49	0.31	0.27	0.27	0.15
G	10.0	0.58	0.59	0.37	0.22	0.32	0.16

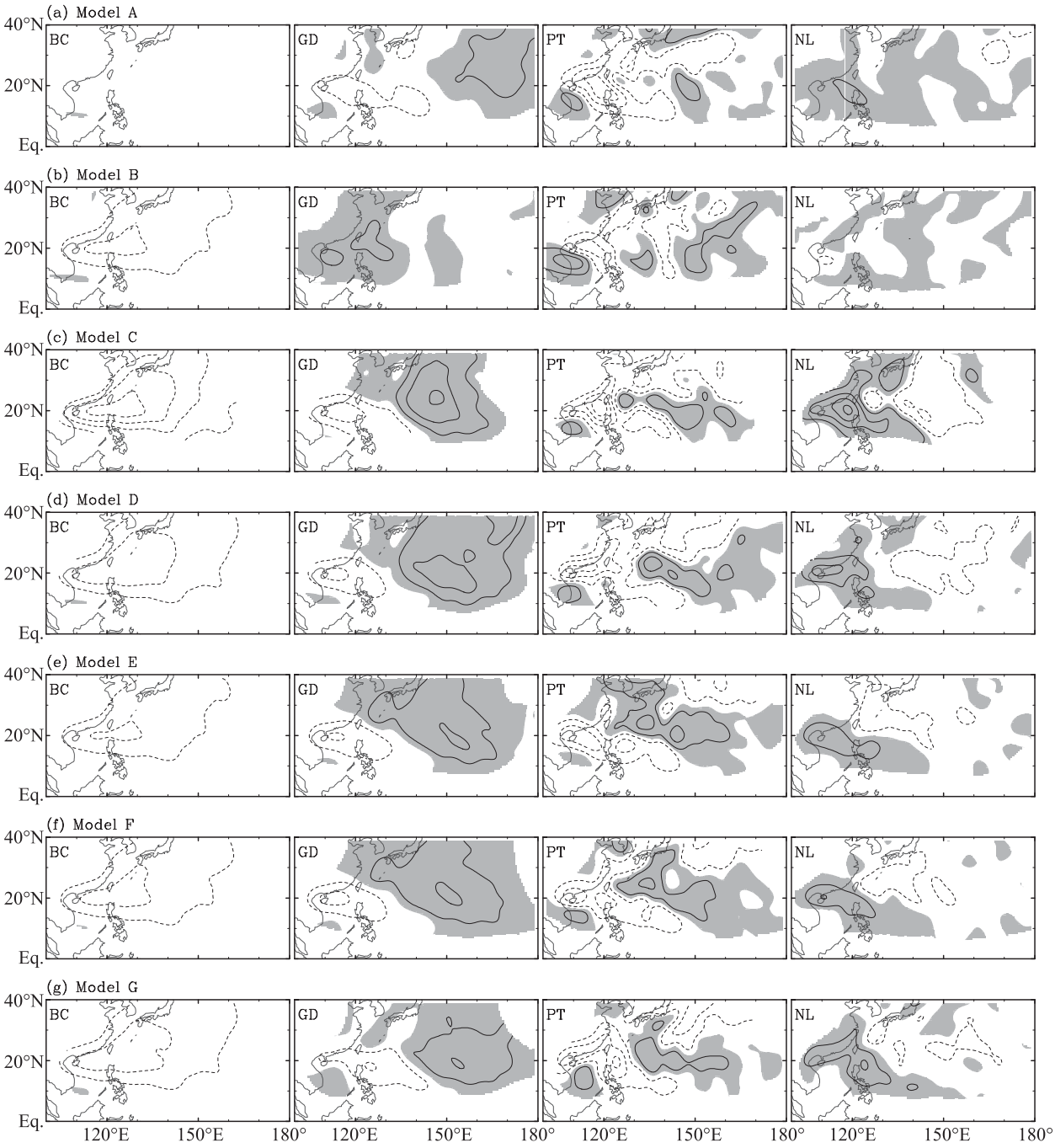

FIG. 2. (a)–(g) BC-, GD-, and PT-bias, and NL contributions to the passage frequency bias of individual models {contours; contour interval is 0.2 $[(2.5° \times 2.5°)^{-1}$ (3-month season)$^{-1}]$, starting with ± 0.1, with solid and dashed contours indicating positive and negative contributions, respectively}. Gray shading represents regions of positive contributions. A 1–2–1 spatial smoothing has been applied each in longitudinal and latitudinal directions.

there is no contour in the figure. This feature reflects the underestimation of the BC in the July–September season (second column of Table 3) compared with the observed climatological count over the 25 years (1979–2003) of 14.3. Yokoi et al. (2009) reported that the deficit of simulated TCs by the five AOGCMs in this season is primarily caused by a bias in the seasonal migration of the monsoon trough in the meridional direction. The GD bias contributes to an overestimation (underestimation) of the passage frequency in the northern and eastern parts

of the domain (the northern SCS) for all of the models except for model B. The GD-bias contribution of model B exhibits a nearly opposite distribution. As for the PT bias, most models have similar features: it contributes to an underestimation over the northern SCS and over and to the east of the Philippines, and an overestimation to the south and east of the area of the underestimation. The NL contribution is generally smaller, except over the northern SCS, which implies that biases in C, g, and p are considerably smaller than the respective observed values for most of the WNP.

To quantify the magnitude of the biases and contributions, we calculate the root-mean-square errors (RMSEs) over the WNP basin, normalized by the spatial standard deviation of the observed passage frequency (Fig. 1h). These metrics are shown in the fourth through eighth columns of Table 3. The two AGCMs (models A and B) exhibit generally smaller RMSEs of the passage frequency (fourth column) than the AOGCMs, which is consistent with the S indices. The differences between the AGCMs and AOGCMs result primarily from the GD-bias contribution, whose RMSE is generally smaller for the AGCMs than the AOGCMs. In contrast, the RMSE of the BC-bias contribution for model B and that of the PT-bias contribution for model A are only comparable to the respective RMSEs for the AOGCMs. This suggests that the reproducibility of the AOGCMs in simulating the TC translation vector and the preferable track is as good as that of the AGCMs, albeit with a low horizontal resolution. In addition, note that the RMSEs of the NL contribution are generally smaller than the other RMSEs, with the exception of model C.

By performing the abovementioned examination of model performance, we decided to use both high-resolution AGCM and medium-resolution AOGCM simulations to perform multimodel future projection, although the models in the latter group exhibit larger biases in the passage frequency, which results mainly from the GD bias.

b. *Future projection*

In this section, we present future projections of the passage frequency and their attribution on a multimodel basis. In this section, we argue that intermodel consistency is obtained from comparison of the seven models, which is only a small sample of dozens of existing GCMs, as mentioned in section 2a. Here, the multimodel ensemble is obtained by a simple averaging over the seven models, unless otherwise stated. Before calculating the ensemble mean, the results of each model are multiplied by the ratio of the observed to simulated BC to eliminate the influence caused by the apparent negative BC bias. The multimodel ensemble of the passage frequency in the current climate experiments (Fig. 3a) reproduces the gross horizontal distribution of the observations, with a maximum found to the southeast of Taiwan and small values in the south and east of the domain.

Figures 3b–f present a multimodel ensemble of the passage frequency change and its attribution as well as their intermodel consistencies. Contours in the figures show future changes and contributions, while color tones indicate how many models project positive future changes and contributions. The horizontal distribution of the passage frequency change (Fig. 3b) is characterized by a gross zonal contrast over the domain. In the tropics, a large increase with consistency is found east of 140°E over the central Pacific, while decreases with moderate consistency are located over the SCS and the Philippine Sea. For East Asian countries, decreases with moderate consistency are found over western Japan and the Korean peninsula, with slight increases found over eastern Japan and central China.

The decomposition of the passage frequency change using the ISTAGL analysis is shown in Figs. 3c–f. The BC-change contribution (Fig. 3c) is negative throughout the domain with a maximum decrease found southeast of Taiwan where the passage frequency has a positive maximum. Apparently, this reflects the decrease of BC. Although this decrease is consistent with a summary given by Knutson et al. (2010) stating that most recent studies project decreases of annual BC, the consistency here is not high; for the July–September season, four models (A, B, C, and E) project decreases while the other three project increases.

The substantial east–west contrast in the passage frequency change appears to be due mainly to the GD-change contribution (Fig. 3d), which exhibits positive contributions over the tropical central Pacific and negative ones to its northwest. The intermodel consistency of these contributions is higher than that of respective passage frequency changes. Six out of seven models project that the passage frequency would decrease because of the GD change over western Japan, the Korean peninsula, and the surrounding oceans. Note that the magnitude of the negative GD-change contribution is comparable to that of the BC-change contribution southeast of Taiwan.

Compared with the BC- and GD-change contributions, the PT-change contribution (Fig. 3e) exhibits a more complicated horizontal distribution and is responsible for the fine structure of the passage frequency change. In particular, positive contributions are found at around 25°N, 150°E and 20°N, 165°E, accompanied by a negative one at around 17.5°N, 155°E. Such a distribution hints at a slight northeastward shift of a ridge of simulated high passage frequency

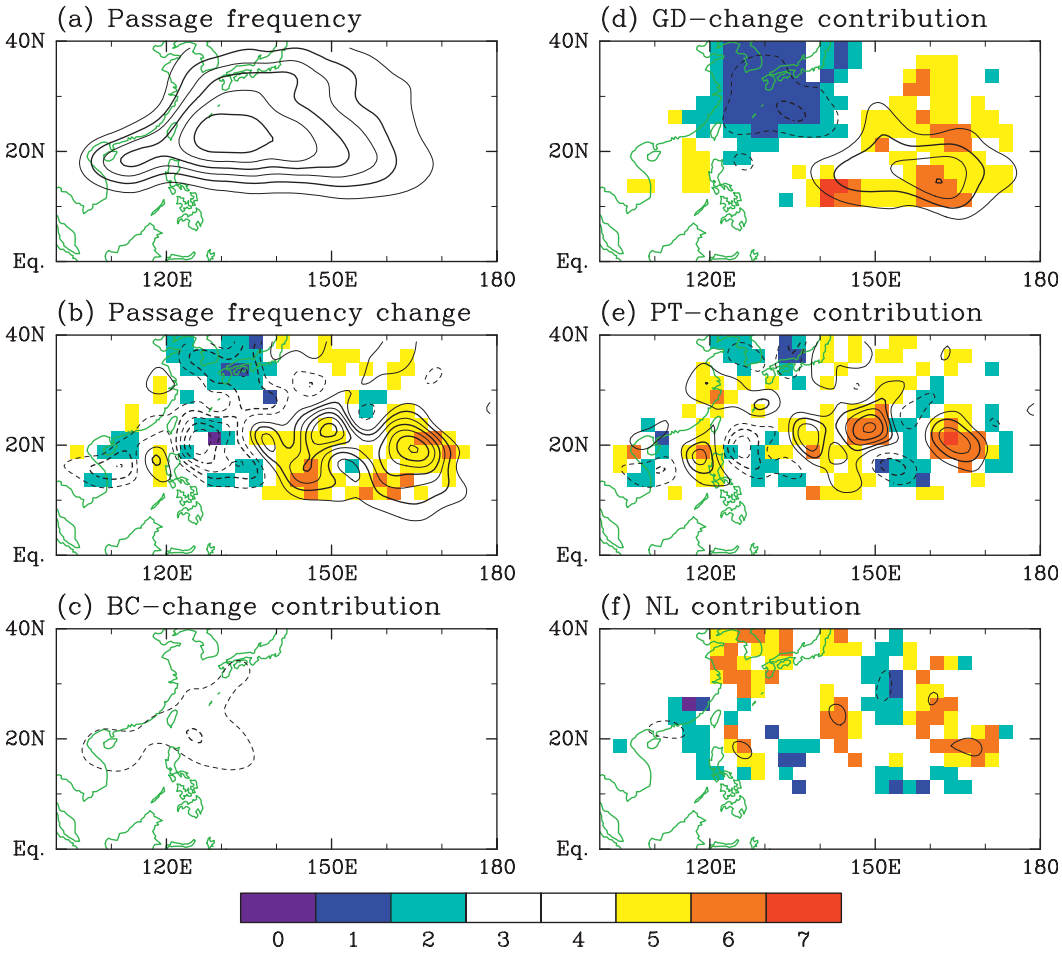

FIG. 3. Multimodel ensembles in (a) passage frequency, (b) future change of passage frequency, (c) BC-, (d) GD-, and (e) PT-change contribution, and (f) NL contribution. The contour interval in (a) is 0.2 $[(2.5° \times 2.5°)^{-1}$ (3-month season$)^{-1}]$ and in (b)–(f) is 0.025 $[(2.5° \times 2.5°)^{-1}$ (3-month season$)^{-1}]$ with zero contours omitted. Solid and dashed contours represent positive and negative changes, respectively. Color shading in (b)–(f) represents how many models project positive changes. A 1–2–1 spatial smoothing has been applied each in longitudinal and latitudinal directions.

extending in a southeast–northwest direction over the central Pacific (Fig. 3a). A pair of positive and negative contributions is also found to the east and west, respectively, of the maximum in passage frequency at around 22.5°N, 130°E, implying a slight eastward shift of the high-frequency area. Over Southeast and East Asian countries, the PT-change contribution is positive with modest intermodel consistency over the northern Philippines, the east coast of China, and eastern Japan, whereas it is negative over western Japan, the Korean peninsula, and the Indochina peninsula.

The NL contribution (Fig. 3f) is considerably less than the other three contribution terms, although its sign is relatively consistent among the models over a wide area. This implies that magnitudes of the projected future changes of C, g, and p are generally small relative to the respective values in the current climate experiments. Therefore, it seems appropriate to discuss the attribution of the passage frequency change in a "linear" framework of the contributions of the BC, GD, and PT changes.

We further examine the attribution of the passage frequency changes, paying special attention to those over Southeast and East Asian countries. Figure 4a indicates seven areas that are considered: the eastern Indochina peninsula (ICP; 10°–20°N, 105°–110°E), the southern coast of China (SCH; 20°–25°N, 105°–117.5°E), the eastern coast of central China (CCH; 26°–35°N, 117.5°–122.5°E), Okinawa (OKI; 25°–30°N, 125°–132.5°E), the Korean peninsula (KOR; 32.5°–40°N, 125°–130°E), western Japan (WJP; 30°–40°N, 130°–137.5°E), and eastern Japan (EJP; 30°–40°N, 137.5°–145°E). The passage frequency changes and three linear contribution terms over the seven areas for individual models are shown in Figs. 4b–h. These

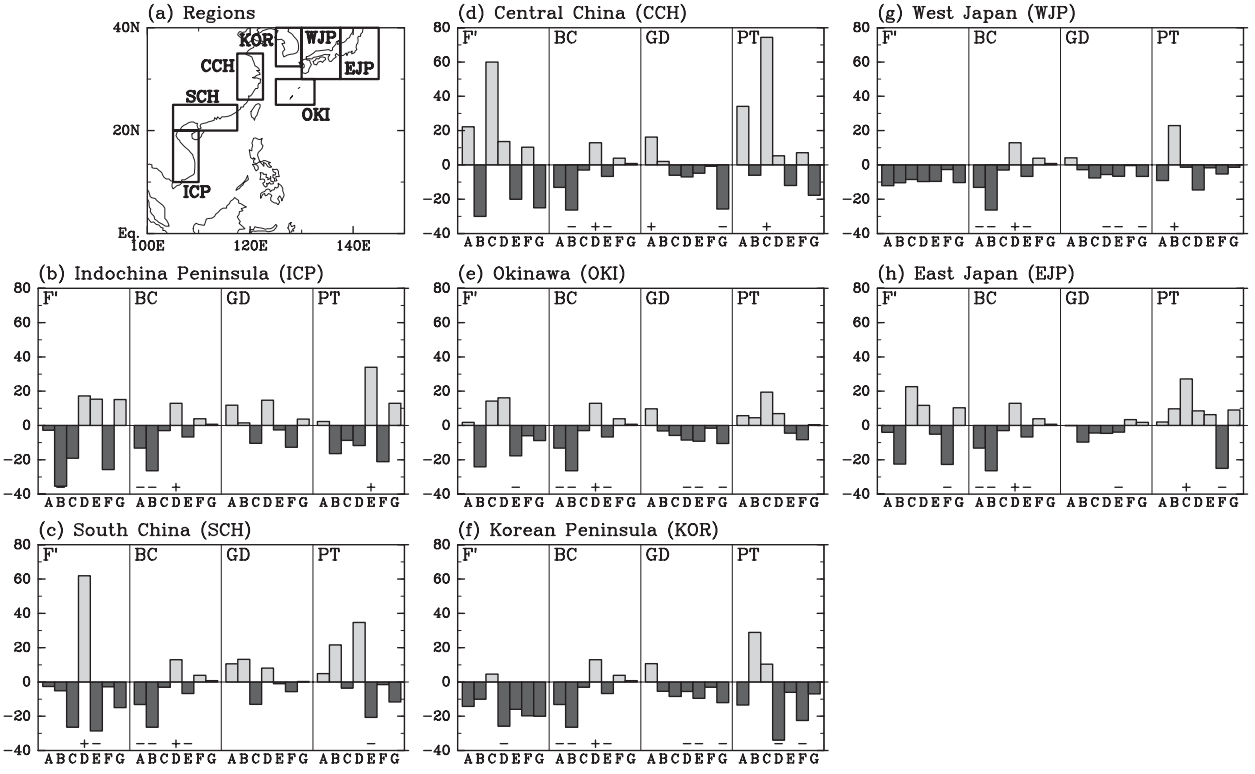

FIG. 4. Fractional future change (i.e., normalized by the passage frequency in the current climate experiment) of passage frequency and its attribution over seven coastal regions. (a) Definition of the regions. (b)–(h) the passage frequency change (i.e., F'), and BC-, GD-, and PT-change contributions for models A–G over the regions. The unit of the y axis is percentage. The plus (minus) symbols indicate that the change and contribution are positive (negative) and statistically significant at the 90% confidence level.

variables are normalized by the local passage frequency in the current climate experiment of individual models to examine the fractional change (as a percentage). Note that the fractional contribution of the BC change is, by definition, independent of the area.

These figures indicate a large intermodel diversity in the sign of the passage frequency change, especially over ICP, CCH, OKI, and EJP, which suggests a difficulty in obtaining reliable future projections of regional passage frequency. Nevertheless, we find several aspects that are qualitatively consistent among most (at least six) of the models. There is modest consistency over WJP. All seven models project decreases of the passage frequency, six models (with the exception of A) project negative GD-change contributions, and six models (with the exception of B) project negative PT-change contributions. The relatively high consistency can also be found in the passage frequency change and GD-change contribution over KOR and the GD-change contribution over the OKI. Furthermore, six and five models project positive contributions of the PT change over the EJP and OKI, respectively.

It is interesting to note that the difference between two AGCMs (A and B) is generally as large as that between an AGCM and an AOGCM, although they employed the same boundary conditions (such as the SST and greenhouse gas concentrations) for the current and future climate experiments, as reported by Murakami et al. (2012b). For example, model A projects a positive GD-change contribution over OKI, KOR, and WJP, whereas model B projects a negative contribution. The sign of the PT-change contribution over ICP, CCH, KOR, and WJP differs between the two models. In addition, with the exception of the BC-change contribution, there is no systematic difference between AGCM and AOGCM groups.

The difference in the future projection of the passage frequency between two AGCMs is at least partly due to projected future changes in environmental conditions over the tropical Pacific that are considered to modulate the behavior of TCs. For example, Fig. 1 of Murakami et al. (2012b) shows differences in the change of climatological mean precipitation. The change projected by model A exhibits a positive maximum just east of the date line, while that projected by model B has two maxima west of the date line and over the eastern Pacific. Associated with this difference, projected future changes in circulation fields are also different between the two

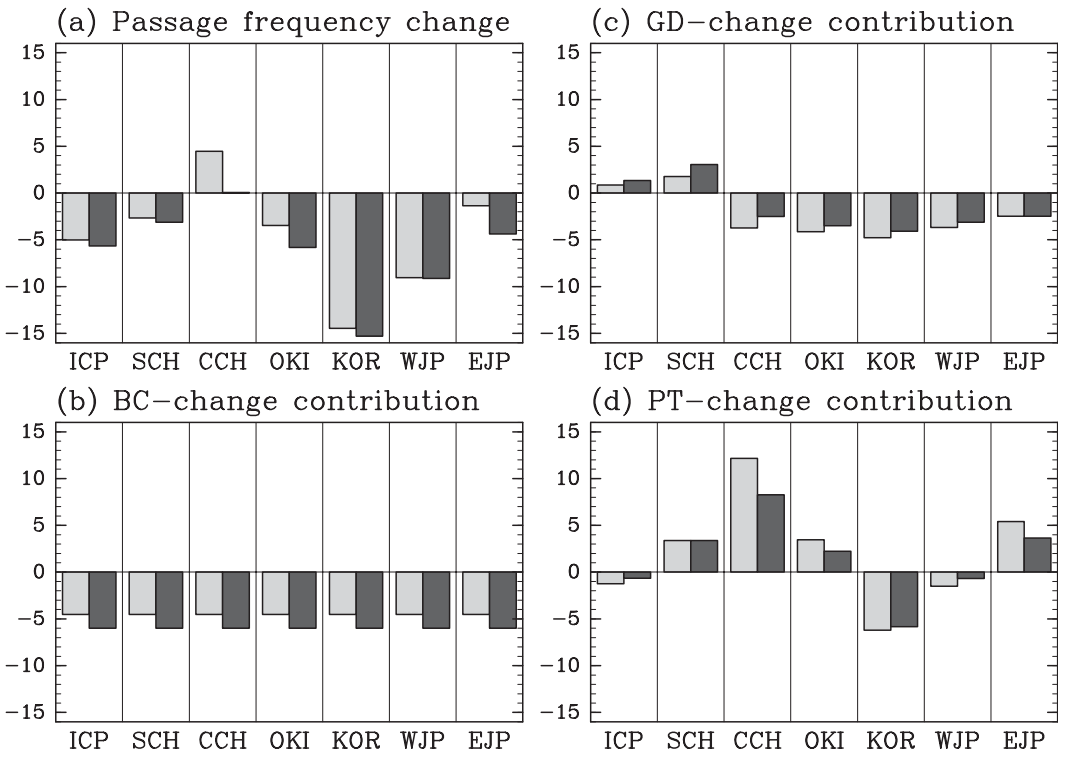

FIG. 5. Multimodel ensembles of (a) fractional passage frequency change, and (b) BC-, (c) GD-, and (d) PT-change contributions over the seven regions indicated in Fig. 4a. The unit of the *y* axis is percentage. Light bars indicate the simple average over the seven models, whereas dark bars indicate the weighted average using the *S* index shown in the third column of Table 3.

AGCMs. Note that Murakami et al. (2012a) pointed out that these differences result from the difference in the representation of the physical processes, such as cumulus parameterization.

To confirm the robustness of the projected future change against the simulated interannual variability, we performed statistical significance tests using a bootstrap method. We randomly divided 50 seasons of AGCM simulations (25 seasons of the current climate and 25 seasons of the future climate experiments) into two 25-season groups to perform the ISTAGL analysis. For the AOGCM experiments, we divided 80 seasons into two 40-season groups. We repeated this procedure 10 000 times to estimate the probability density function that is used as a reference for evaluating the significance of the change. Plus and minus symbols in Fig. 4 indicate that the changes are positive and negative, respectively, and are statistically significant at the 90% confidence level. The negative BC-change contributions by models A, B, and E and the positive one by model D are generally significant. For the GD-change contribution, the most peculiar feature is that models D, E, and G project significantly negative contributions over three areas, OKI, KOR, and WJP. In contrast to these two contributions, the PT-change contribution is generally less significant, while that over KOR is significant for two models (D and F). As for the passage frequency changes, only 5 out of the 49 tests (7 models times 7 regions) pass the 90% confidence level, which seems no different from random. This further indicates the difficulty in assessing change in regional passage frequency. Furthermore, the number of significant changes is less than that of the three contribution terms. This implies that cancellation of the three contributions, some of which are statistically significant, may result in insignificant passage frequency changes.

Multimodel ensembles of passage frequency changes and their attributions are shown in Fig. 5. We adopt two types of weights for calculation of the ensemble. The light gray bars represent the simple seven-model average, while dark gray bars represent the weighted average using the *S* index shown in Table 3 to account for the models' performance in simulating the passage frequency. The two multimodel ensembles considerably resemble each other.

The projected changes in passage frequency exhibit large differences between the areas, ranging from a nearly 15% decrease over the KOR to an increase of

a few percent over the CCH. The BC-change contribution is independent of the area, as mentioned above, and results in an approximately 5% decrease in the passage frequency. The GD-change contribution is negative and comparable to the BC-change contribution over CCH, OKI, KOR, WJP, and EJP, and is slightly positive over ICP and SCH, consistent with Fig. 3d. The PT-change contribution exhibits a large regional diversity and mostly explains the regional difference in the change in passage frequency. The maximum negative contribution is found over KOR with more than a 5% decrease, whereas the maximum positive contribution is found over the CCH with approximately a 10% increase. Negative contributions over ICP, KOR, and WJP and positive ones over the other regions are consistent with Fig. 3e. In particular, the increase in the passage frequency over the CCH is solely caused by the PT change.

c. *Reasons for the GD-change contributions*

The overall negative contributions of the GD change over and around East Asian countries and positive ones east of 140°E over the tropical central Pacific can be understood by examining zonal distributions in the future change of genesis frequency. In the current climate, TCs are frequently generated over the northern SCS and Philippine Sea south of 25°N. As reported by Yokoi and Takayabu (2009) and Murakami et al. (2011, 2012b), all seven models project that this main development region would either extend or shift eastward. Figure 6 shows the longitudinal distribution of future changes in the genesis frequency projected by the seven individual models represented by letters and lines as well as a simple seven-model ensemble represented by bars. Note that the zonal mean of the change has been subtracted, and thus this figure directly plots the GD change. Ensemble averages exhibit increases east of 150°E accompanied by decreases over 120°–150°E.

The increases in the former region apparently contribute to the increase in the local passage frequency. In addition to the local contribution, there exists a remote contribution of the GD change. Most TCs generated in the former region tend to recurve at around 140°E and then to be translated in a northeastward direction over the seas east of Japan, whereas a large portion of TCs generated in the latter region are translated northwestward toward East Asian countries. As a result, the zonal contrast in the GD change contributes to decreases in the passage frequency over and around the East Asian countries.

The increase in TC genesis over the central Pacific is considered to result from an El Niño–like horizontal pattern in tropical SST trends (Yokoi and Takayabu 2009). Furthermore, El Niño–like trends are also

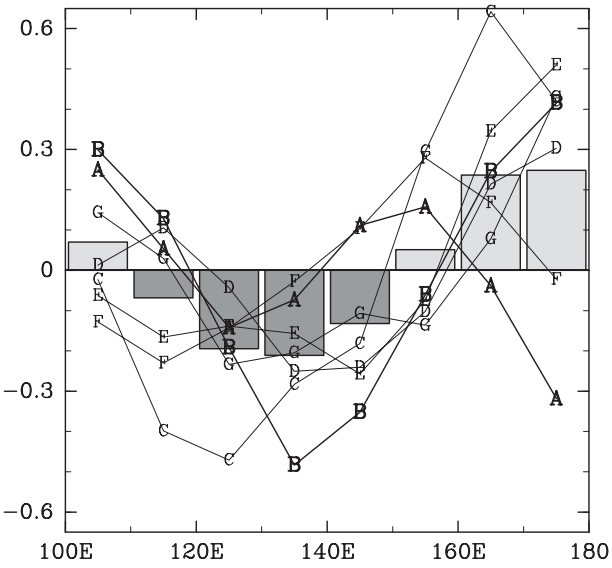

FIG. 6. Longitudinal distribution of the future change of the genesis frequency for individual models (indicated by letters and lines) and multimodel ensembles (bars). The unit is the number of TCs generated in the 40° × 10° latitude–longitude grid over one season. Note that the contribution from the BC change has been removed by subtracting the zonally averaged changes.

projected by most CMIP3 AOGCMs (Yamaguchi and Noda 2006; Meehl et al. 2007b). Meehl et al. (2007b) demonstrated that 13 out of 16 CMIP3 AOGCMs exhibit a positive correlation pattern over the equatorial Pacific between the simulated SST anomaly related to El Niño and projected SST trends. This suggests that the zonal contrast in the GD change (and, by extension, its contribution to the passage frequency change) is considered to be probable from the viewpoint of the intermodel agreement.

It should also be noted that the extent of the eastward shift of the main development region is smaller for model A than for the other models. While model A projects a decrease of GD in 120°–140°E, its accompanying increase is found in 140°–160°E, where generated TCs tend to be translated toward the Korean peninsula and Japan. As a result, this model exhibits a positive GD-change contribution over the OKI, KOR, and WJP regions, whereas the other models project negative ones. This suggests that although most recent studies project an eastward shift of the main development region (Yokoi and Takayabu 2009; Li et al. 2010; Murakami et al. 2011, 2012b), landfall frequency for a certain country depends strongly on the extent of the eastward shift, for which the intermodel diversity is still large, as can be inferred from Fig. 6. This suggests the difficulty of obtaining future projections of TC activity at a regional scale.

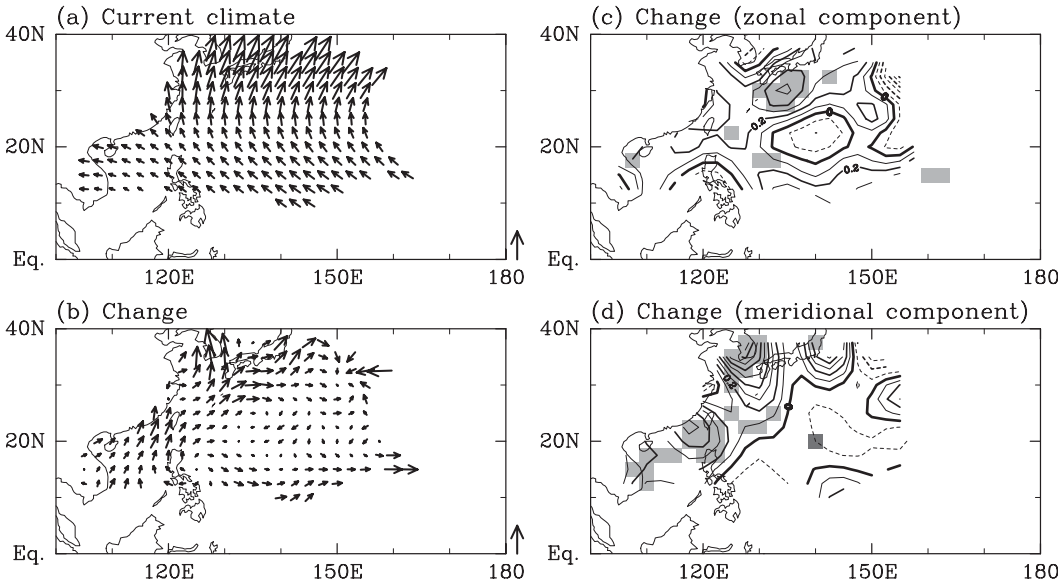

FIG. 7. Multimodel ensembles of simulated mean TC translation vector in (a) current climate experiments (reference vector represents 10 m s^{-1}), (b) the future change (reference vector represents 1 m s^{-1}), and the (c) zonal and (d) meridional component of the change (contours; contour interval is 0.1 m s^{-1}). Light and dark shading in (c) and (d) indicate that more than five models project positive and negative changes, respectively.

d. Reasons for the PT-change contributions

Figures 3e and 5d show that the PT-change contribution is negative over KOR and WJP, whereas it is positive to their east (EJP) and west (CCH). This regional contrast can be interpreted from the viewpoint of future changes in the mean translation velocity of TCs. Figure 7a shows the horizontal distribution of the ensemble-mean translation vector for the current climate simulation. The vectors point in a northwestward direction in the tropical WNP south of 25°N, and point in a northward and northeastward direction to its north. Over the SCS, the vector generally points in westward and west-northwestward directions. These features agree well with the observations. The ensemble-mean future change is shown in Fig. 7b. In general, the translation vector shifts to the right over oceanic areas surrounding Southeast and East Asian countries, with the exception of KOR. To the south of Japan, more than five models project that the translation vector points in a more eastward direction (Fig. 7c). This suggests that TCs that tend to translate northward over this area toward KOR and WJP in the current climate would take a more eastward direction in the future climate, and some of them would reach EJP instead. Because the passage frequency over the region south of Japan is higher than over other regions at the same latitude (Figs. 1h and 3a), the change in the translation vector shifts the high passage frequency ridge eastward, resulting in positive PT-change contributions over EJP and negative ones over KOR and WJP. Furthermore, the translation change vector converges around CCH and OKI, which seems consistent with the positive PT-change contribution over these regions.

Over the SCS, more than five models project that the translation points in a more northward direction (Fig. 7d), resulting in negative and positive PT-change contributions over the ICP and SCH, respectively. Furthermore, in general, the translation vector changes over the tropical central Pacific and in the region east of the Philippines points in an eastward direction, seemingly also consistent with the northeastward shift of the high passage frequency ridge and the eastward shift of the region with maximum passage frequency. In contrast, projected changes in the translation vector point northward over KOR, which can be considered to contribute to the acceleration of the northward translation, but not a change in direction.

The most important factor that affects the mean translation vector is considered to be the steering flow, which is the environmental flow averaged over the deep troposphere (George and Gray 1976). Many studies have attributed the observed translation vector variability and projected future changes to those in the steering flow (Ho et al. 2004; Kim et al. 2005; YT; Murakami et al. 2011). In this paper, the steering flow is defined as the mass-weighted vertical average of horizontal wind between the 850- and 300-hPa levels. Its projected future changes are found to be consistent with the changes in the mean translation vector in several regions. Figure 8a presents a seven-model ensemble of future changes to the zonal

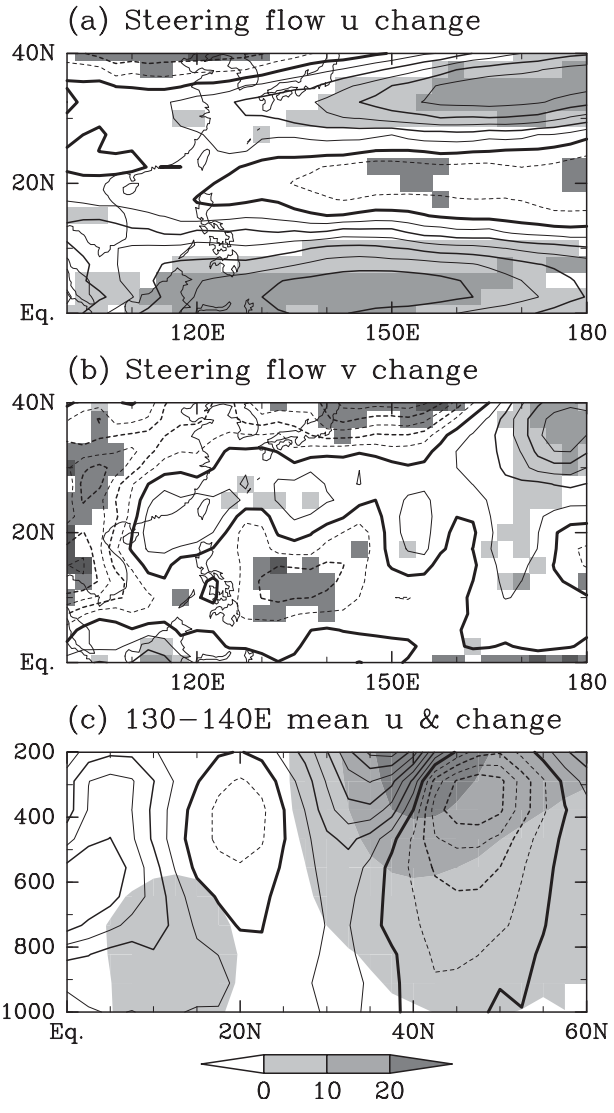

FIG. 8. Multimodel ensembles of future changes in July–September environmental flow. (a) Changes in zonal components of the steering flow (contours; contour interval of $0.15\,m\,s^{-1}$). (b) As in (a), but for the meridional component (contours; contour interval of $0.05\,m\,s^{-1}$). In these panels, the darkest and second darkest shading indicate that seven and six models project negative changes, respectively, while the second lightest and lightest shadings indicate that seven and six models project positive changes, respectively. (c) Latitude–height cross section of zonal wind averaged over 130°–140°E in the current climate experiments (shading) and its future change (contours; contour interval is $0.25\,m\,s^{-1}$). In all panels, the thickest line indicates the zero contour and the other solid (dashed) contours indicate positive (negative) values.

components of the steering flow. In the midlatitudes, the zonal flow change exhibits a positive maximum located at around 35°N, 170°E, and positive changes with intermodel consistency expand to the west-southwest toward the oceanic area south of Japan. These changes indicate a strengthening (weakening) of westerly (easterly) flow, which is considered to be responsible for the projected eastward veer of the mean translation vector shown in Figs. 7b and 7c. Note that the magnitude in the zonal flow change is smaller over the East China Sea. In addition, the zonal flow change over the tropical WNP south of 15°N is also positive and consistent with the translation vector change.

The vertical structure of the westerly flow change is presented in Fig. 8c. In the current climate experiments, the subtropical jet is reproduced with its axis at 40°N at the 200-hPa level and is consistent with the observations. The ensemble-mean zonal wind change in the midlatitudes exhibits a quasi-barotropic structure with positive values at around 25°–40°N and negative values at around 40°–55°N. The former corresponds to the positive steering flow change in Fig. 8a. This north–south contrast implies that the subtropical jet axis would shift in a southward direction.

Not only the present seven models but also most of the other CMIP3 AOGCMs project such changes in the subtropics and midlatitudes. To demonstrate this, we analyze outputs of twentieth-century climate experiments and SRES A1B scenario experiments of 15 other CMIP3 models (Table 2) in addition to the five CMIP3 models examined thus far (C–G). Figure 9a shows the ensemble-mean changes in the zonal component of the steering flow. As in Fig. 8a, a southward shift of the subtropical westerly jet is projected, with positive changes found in 25°–35°N and negative changes to its north. Not only the ensemble mean but also 16 out of 20 CMIP3 models project positive changes over 25°–35°N, 130°–160°E (Fig. 9b). These projections are basically consistent with those of Kosaka and Nakamura (2011). They showed that the CMIP3 multimodel ensemble exhibited positive zonal wind changes at 30°–45°N for the 200-hPa level and 25°–40°N for the 850-hPa level in the June–August season, one month earlier than the season targeted in this paper. Therefore, it can be said that the projected westerly flow changes to the south of the subtropical jet axis and, by extension, the associated eastward veer of the translation vector are probable in the context of intermodel consistency. Therefore, the negative PT-change contribution over KOR and WJP and the positive one over EJP may also be probable.

Over northern SCS and in the area around Taiwan, the ensemble-mean steering flow change is southerly (Fig. 8b). This may be related to the projected northward veer of the translation vector (Figs. 7b,d). However, the southerly change of the flow is not consistent among the models, and further discussion of individual models may be necessary, which remains for our future study.

Note that the steering flow change does not fully explain the mean TC translation change. For example, the

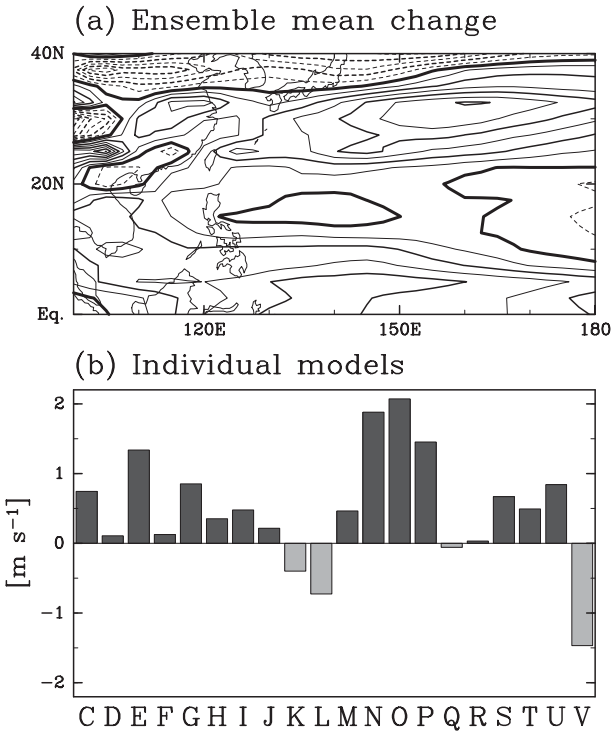

FIG. 9. (a) Multimodel ensembles of July–September future changes in the zonal component of the steering flow for 20 CMIP3 AOGCMs (contours; contour interval is 0.15 m s^{-1}, with dashed contours indicating negative values). (b) Future changes (m s^{-1}) of the zonal component of the steering flow averaged over 25°–35°N, 130°–160°E projected by individual CMIP3 AOGCMs. The models include C–G (see Table 1), as well as those provided in Table 2.

meridional component of the steering flow change is negative over the East China Sea and east of Japan, which is inconsistent with the projected northward veer of the translation vector (Figs. 7b,d). In addition to the steering flow, the horizontal and vertical shear of environmental flow may affect the TC translation (e.g., Wang and Li 1995; Wu and Emanuel 1993). Nonlinearity of TCs is considered to move TCs themselves northward or northwestward, which is known as beta drift (e.g., Holland 1983). Projected future changes of the shear and the mean nonlinearity would explain the mean TC translation change that cannot be explained by the steering flow change, which we also want to remain for our future study.

4. Conclusions

Because of the severe impact of TCs on society, how global warming would influence the frequency of TC landfall is a direct concern for local populations. While we can perform future projection of the regional passage frequency through the direct approach, it is sometimes difficult to discuss causes of its changes and evaluate their credibility and uncertainty, because the passage frequency is influenced by three aspects of TC statistical behavior: BC, GD, and PT. Each aspect is in turn influenced by particular aspects of environmental circulation fields. In this paper, we demonstrate that the decomposition of the passage frequency change into the contribution of BC, GD, and PT changes facilitates the discussion. We further show that the ISTAGL analysis proposed by YT successfully accomplishes the decomposition and is therefore a valuable method that can be utilized in studies taking the direct approach to future projections of TC activity.

We perform future projections of the regional passage frequency over the WNP on a multimodel basis, by analyzing track data of TC-like disturbances simulated in the current and future climate experiments of the two high-resolution AGCMs and five medium-resolution AOGCMs. Before making future projections, we evaluate the models' performance in simulating the passage frequency and attribute its biases. The bias is generally smaller for the AGCMs than the AOGCMs, presumably because the AGCMs have much higher horizontal resolutions than the AOGCMs, and the AGCMs utilize the observed SST as a boundary condition so that they can simulate environmental fields that modulate TC behavior more realistically than the AOGCMs. Decomposition of the bias reveals that the GD-bias contribution plays the most essential role in the contrast between the AGCMs and AOGCMs. The BC- and PT-bias contributions are considerably smaller for one of the AGCMs (A and B, respectively), while the contributions of the other AGCM is only comparable to those of the AOGCMs.

Despite considerable intermodel diversity, some aspects of projected future changes of the passage frequency and their attribution are considered to be consistent among most of the seven models. The multimodel ensemble projects that the passage frequency would increase over the tropical central Pacific east of 140°E and decrease to its west and northwest. While the BC change contributes to a decrease of the passage frequency over the entire WNP basin, the general horizontal contrast is responsible for the GD-change contribution. As reported by Yokoi et al. (2009) and Murakami et al. (2011, 2012b), the seven GCMs studied here project similar patterns in the genesis frequency change in that the main development region located around the Philippines would extend, or even shift, eastward, probably because of El Niño–like pattern of the SST change. Because of this consistent GD change, the passage frequency would increase in the southeastern part of the WNP basin, whereas it would decrease in the western and northwestern parts.

In addition, the negative GD-change contributions are statistically significant for three GCMs. Note, however, that the extent of the eastward shift differs from one model to another, resulting in diversity in the GD-change contributions. This implies difficulty of the regional passage frequency projection.

The PT-change contribution is responsible for the detailed horizontal distribution of the passage frequency changes. In areas around the landmasses, the PT change would decrease the passage frequency over WJP, KOR, and ICP, whereas it would increase the passage frequency over EJP and CCH. In particular, because of the PT change, the passage frequency would increase by approximately 10% over CCH and 5% over the EJP, whereas it would decrease by more than 5% over KOR. These changes are attributable to the changes in TC translation vector. The TCs would take a more northerly track over the SCS and near Taiwan, and they would take a more easterly track over the region south of Japan. The latter shift is considered to be from the projected southward shifts in the subtropical jet axis.

While some of the projections are consistent among the seven models, it seems premature to argue their reliability from the viewpoint of intermodel consistency, because the multimodel projection using the seven models covers only a limited part of the intermodel diversity in projections of dozens of existing GCMs. Instead of extend our direct approach to other GCMs, here we argue that the projections of the environmental conditions that are considered to cause GD and PT changes are consistent with projections of other GCMs. Yamaguchi and Noda (2006) and Meehl et al. (2007b) reported that the majority of the CMIP3 models project the El Niño–like SST changes. This consistency suggests that the GD change (and, by extension, its contribution to the passage frequency change) is considered to be probable from the viewpoint of intermodel agreement. Furthermore, the southward shift of the subtropical jet is also projected by the majority (16) of the 20 CMIP3 models, which implies the reliability of the PT-change contribution over and around Japan to a certain degree.

This paper examines the future change in the climatological (25- and 40-yr) mean passage frequency over the WNP. On the other hand, a number of studies have pointed out that the activity is affected considerably by El Niño–Southern Oscillation (ENSO) (e.g., Chan 2000; Kim et al. 2011; Li and Zhou 2012), which is further modulated with decadal time scales (Ashok et al. 2007; Wang et al. 2009). Because the statistical behavior of ENSO would also change in the future climate (Yeh et al. 2009; Collins et al. 2010), it may be important to assess its impacts on the mean TC activity, which we want to remain for our future study.

Recently, a number of next generation AOGCM and AGCM experiments have been performed under the CMIP5 and other projects. It is quite important to extend our analyses using these newly released outputs to investigate intermodel diversity more in detail, which we intend to do in the future.

Acknowledgments. The authors acknowledge the modeling groups, PCMDI, and World Climate Research Program's Working Group on Coupled Modeling for their roles in making the CMIP3 multimodel dataset available. Support of this dataset is provided by the Office of Science, U.S. Department of Energy. The ''Data Integration and Analysis System'' Fund for National Key Technology from the Ministry of Education, Culture, Sports, Science and Technology (MEXT), Japan, supported the authors in obtaining the dataset. The authors are also grateful to the Japan Meteorological Agency for provision of the best-track data. This study is supported by the Environment Research and Technology Development Fund (S-5-2 and A1201) of the Ministry of the Environment, Japan, and the ''Projection of the Change in Future Weather Extremes Using Super-High-Resolution Atmospheric Models'' project supported by the KAKUSHIN program of MEXT, Japan. Calculations using the AGCMs were performed on the Earth Simulator.

REFERENCES

Ashok, K., S. K. Behera, S. A. Rao, H. Weng, and T. Yamagata, 2007: El Niño Modoki and its possible teleconnection. *J. Geophys. Res.,* **112,** C11007, doi:10.1029/2006JC003798.

Chan, J. C. L., 2000: Tropical cyclone activity over the western North Pacific associated with El Niño and La Niña events. *J. Climate,* **13,** 2960–2972.

Collins, M., and Coauthors, 2010: The impact of global warming on the tropical Pacific Ocean and El Niño. *Nat. Geosci.,* **3,** 391–397.

Flato, G. M., G. J. Boer, W. G. Lee, N. A. McFarlane, D. Ramsden, M. C. Reader, and A. J. Weaver, 2000: The Canadian Centre for Climate Modeling and Analysis global coupled model and its climate. *Climate Dyn.,* **16,** 451–467.

George, J. E., and W. M. Gray, 1976: Tropical cyclone motion and surrounding parameter relationship. *J. Appl. Meteor.,* **15,** 1252–1264.

Gordon, H. B., and Coauthors, 2002: The CSIRO Mk3 Climate System Model. CSIRO Atmospheric Research Tech. Paper 60, 130 pp.

Gualdi, S., E. Scoccimarro, and A. Navarra, 2008: Changes in tropical cyclone activity due to global warming: Results from a high-resolution coupled general circulation model. *J. Climate,* **21,** 5204–5228.

Ho, C.-H., J.-J. Baik, J.-H. Kim, D.-Y. Gong, and C.-H. Sui, 2004: Interdecadal changes in summertime typhoon tracks. *J. Climate,* **17,** 1767–1776.

Holland, G. J., 1983: Tropical cyclone motion: Environmental interaction plus a beta effect. *J. Atmos. Sci.,* **40,** 328–342.

Kim, H.-M., P. J. Webster, and J. A. Curry, 2011: Modulation of North Pacific tropical cyclone activity by three phases of ENSO. *J. Climate,* **24,** 1839–1849.

Kim, J.-H., C.-H. Ho, C.-H. Sui, and S. K. Park, 2005: Dipole structure of interannual variations in summertime tropical cyclone activity over East Asia. *J. Climate,* **18,** 5344–5356.

Knutson, T. R., and Coauthors, 2010: Tropical cyclones and climate change. *Nat. Geosci.,* **3,** 157–162, doi:10.1038/ngeo779.

Kosaka, Y., and H. Nakamura, 2011: Dominant mode of climate variability, intermodel diversity, and projected future changes over the summertime western North Pacific simulated in the CMIP3 models. *J. Climate,* **24,** 3935–3955.

Li, R. C. Y., and W. Zhou, 2012: Changes in western Pacific tropical cyclone associated with the El Niño–Southern Oscillation cycle. *J. Climate,* **25,** 5864–5878.

Li, T., M. Kwon, M. Zhao, J.-S. Kug, J.-J. Luo, and W. Yu, 2010: Global warming shifts Pacific tropical cyclone location. *Geophys. Res. Lett.,* **37,** L21804, doi:10.1029/2010GL045124.

LinHo, and B. Wang, 2002: The time–space structure of the Asian–Pacific summer monsoon: A fast annual cycle view. *J. Climate,* **15,** 2001–2019.

Meehl, G. A., C. Covey, T. Delworth, M. Latif, B. McAvaney, J. F. B. Mitchell, R. J. Stouffer, and K. E. Taylor, 2007a: The WCRP CMIP3 multimodel dataset: A new era in climate change research. *Bull. Amer. Meteor. Soc.,* **88,** 1383–1394.

——, and Coauthors, 2007b: Global climate predictions. *Climate Change 2007: The Physical Science Basis,* S. Solomon et al., Eds., Cambridge University Press, 747–845.

Mizuta, R., and Coauthors, 2006: 20-km-mesh global climate simulations using JMA-GSM model: Mean climate states. *J. Meteor. Soc. Japan,* **84,** 165–185.

——, and Coauthors, 2012: Climate simulations using the improved MRI-AGCM with 20-km grid. *J. Meteor. Soc. Japan,* **90A,** 233–258.

Murakami, H., B. Wang, and A. Kitoh, 2011: Future change of western North Pacific typhoons: Projection by a 20-km-mesh global atmospheric model. *J. Climate,* **24,** 1154–1169.

——, R. Mizuta, and E. Shindo, 2012a: Future changes in tropical cyclone activity projected by multi-physics and multi-SST ensemble experiments using the 60-km-mesh MRI-AGCM. *Climate Dyn.,* **39,** 2569–2584.

——, and Coauthors, 2012b: Future changes in tropical cyclone activity projected by the new high-resolution MRI-AGCM. *J. Climate,* **25,** 3237–3260.

Oouchi, K., J. Yoshimura, H. Yoshimura, R. Mizuta, S. Kusunoki, and A. Noda, 2006: Tropical cyclone climatology in a global-warming climate as simulated in a 20-km-mesh global atmospheric model: Frequency and wind intensity analyses. *J. Meteor. Soc. Japan,* **84,** 259–276.

Roeckner, E., and Coauthors, 2003: The atmospheric general circulation model ECHAM5. Part I: Model description. Max Planck Institute for Meteorology Rep. 349, 127 pp.

Sugi, M., A. Noda, and N. Sato, 2002: Influence of the global warming on tropical cyclone climatology: An experiment with the JMA global model. *J. Meteor. Soc. Japan,* **80,** 249–272.

——, H. Murakami, and J. Yoshimura, 2009: A reduction in global tropical cyclone frequency due to global warming. *SOLA,* **5,** 164–167.

Taylor, K. E., 2001: Summarizing multiple aspects of model performance in a single diagram. *J. Geophys. Res.,* **106** (D7), 7183–7192.

——, R. J. Stouffer, and G. A. Meehl, 2012: An overview of CMIP5 and the experiment design. *Bull. Amer. Meteor. Soc.,* **93,** 485–498.

Wang, B., and X. Li, 1995: Propagation of a tropical cyclone in meridionally varying zonal flows: An energetics analysis. *J. Atmos. Sci.,* **52,** 1421–1433.

Wang, X., D. Wang, and W. Zhou, 2009: Decadal variability of twentieth-century El Niño and La Niña occurrence from observations and IPCC AR4 coupled models. *Geophys. Res. Lett.,* **36,** L11701, doi:10.1029/2009GL037929.

Wu, C.-C., and K. A. Emanuel, 1993: Interaction of a baroclinic vortex with background shear: Application to hurricane movement. *J. Atmos. Sci.,* **50,** 62–76.

Yamaguchi, K., and A. Noda, 2006: Global warming patterns over the North Pacific: ENSO versus AO. *J. Meteor. Soc. Japan,* **84,** 221–241.

Yeh, S.-W., J.-S. Kug, B. Dewitte, M.-H. Kwon, B. P. Kirtman, and F.-F. Jin, 2009: El Niño in a changing climate. *Nature,* **461,** 511–514; Corrigendum, **462,** 674.

Yokoi, S., and Y. N. Takayabu, 2009: Multimodel projection of global warming impact on tropical cyclone genesis frequency over the western North Pacific. *J. Meteor. Soc. Japan,* **87,** 525–538.

——, and ——, 2013: Attribution of decadal variability in tropical cyclone passage frequency over the western North Pacific: A new approach emphasizing the genesis location of cyclones. *J. Climate,* **26,** 973–987.

——, ——, and J. C. L. Chan, 2009: Tropical cyclone genesis frequency over the western North Pacific simulated in medium-resolution coupled general circulation models. *Climate Dyn.,* **33,** 665–683.

Zhao, M., I. M. Held, S.-J. Lin, and G. A. Vecchi, 2009: Simulations of global hurricane climatology, interannual variability, and response to global warming using a 50-km resolution GCM. *J. Climate,* **22,** 6653–6678.